Proceedings of the ASME 2022 International Design Engineering Technical Conferences and Computers and Information in Engineering Conference
IDETC 2022
August 14-17, 2022, St. Louis, Missouri, USA

IDETC2022-89625

DESIGN, ANALYSIS, AND PROTOTYPING OF A NOVEL SINGLE DEGREE-OF-FREEDOM INDEX FINGER EXOSKELETON MECHANISM

Wenda Xu
Robotics and Mechatronics Lab
Mechanical Engineering Department
Virginia Tech,
Blacksburg, Virginia 24061

Yujiong Liu
Robotics and Mechatronics Lab
Mechanical Engineering Department
Virginia Tech,
Blacksburg, Virginia 24061

Pinhas Ben-Tzvi *
Robotics and Mechatronics Lab
Mechanical Engineering Department
Virginia Tech,
Blacksburg, Virginia 24061

ABSTRACT

This paper presents a novel index finger exoskeleton mechanism for patients who suffer from brachial plexus injuries, which takes advantage of our previously proposed rigid coupling hybrid mechanism (RCHM) concept used for robotic tail mechanisms. The core idea of this concept is to drive the (i+1)-th link using the motions of the i-th link, instead of the traditional way of transmitting motion directly from the base. This specific configuration allows designing a single degree of freedom (DOF) bending mechanism using a low-profile rack and pinion mechanism and makes the proposed exoskeleton system compact, lightweight, and portable, which are highly desired features for daily usages of exoskeleton gloves. The mechanism is optimized to mimic the grasping motions of human fingers and the sensitivity analysis of its critical design variables is then conducted to explore the performance of the optimization results. The results show that for the current design, the tip position accuracy is mainly affected by the distance between the rack and the corresponding joints. A proof-of-concept prototype was built to verify the novel mobility of the proposed mechanism and to evaluate its performance on a human finger. The index finger exoskeleton experiments demonstrate the new mechanism's ability to grasp small objects.

1 INTRODUCTION

The brachial plexus is a network of nerves that transfers motor function and sensation signals to the shoulder, arm, hand, and fingers. Impairments of such area can result in losing muscle control and/or sensations in the arm, hand, or wrist. One study [1] reports that most of the patients are young males who get injured from traffic accidents, sports, incised wounds, gunshot, carrying a heavy backpack, inappropriate operative positioning, etc. Another research [2] shows that the prevalence rate of this disease is about 1.2% after multiple traumatic injuries and the annual incidence is about 1.64 cases out of a population of 100,000. Studies have found that although the shoulder and the arm function could be restored by surgical operations, the sensation and mobility to the wrist and hand are difficult to be recovered, due to the long distance of the working nerves from the injure zone to the target [3].

Wearable devices can assist patients to perform intensive and repetitive movements to improve their hand motor functions [4–6], and thus are becoming a promising approach to restore the activities of daily living (ADL) of the patients. Therefore, in the past decades, various robotic rehabilitation hand exoskeletons have been developed, among which 102 devices are declared as rehabilitation tools and half are classified as daily assistive tools [7]. Compared to a stationary device [8, 9], a wearable device is one of the most popular daily assistive tools that is designed to be worn for a long period of time and assist the patients to complete their simple ADL. Therefore, besides the basic functionality requirements, demands for new exo-gloves with a reduced size, reduced weight, and increased comfort and durability become more important.

For this purpose, a number of hand rehabilitation designs following alternative approaches are proposed. A soft robotic glove is one of these approaches that recently started drawing researchers' attentions [10–13], due to their reduced number of de-

*Corresponding author – bentzvi@vt.edu

grees of freedom, good wearability (compliant materials), and a low cost. However, these design innovations cannot avoid using thick inflatable segments over the fingers to achieve bending motion. Moreover, these gloves usually require using air compressors and air tanks to operate, which limits portability and user mobility [14] of the glove. Similarly, these shortcomings exist in other robotic gloves driven by hydraulic or pneumatic actuators. Cable-driven and Bowden-driven gloves, such as SAFER [15], CyberGrasp [16], and RAS system [17], use a soft glove mechanism without rigid frames to help restore hand functionalities. However, this design brings in additional issues for the robotic glove, such as uncomfortable pre-tensioning, unexpected shear forces caused by broken cables/tendons, and bulky actuation units mounted on the back of the hand, which decrease the wearability of the glove significantly. The Bravo [18] and the Hope4Care [19] gloves use linkages to transmit the motion. However, they both turned out to be bulky.

Given the shortcomings of the existing wearable robotic glove devices, we propose a novel index finger exoskeleton mechanism which has a compact form factor, safe, low-cost, and user-friendly design. The mechanism is derived from the rigid coupling hybrid mechanism (RCHM) [20, 21] concept with a focus on using one degree of freedom (DOF) to achieve a large range of motion for the index finger. To achieve better grasping performance and comfort, the dimensions of the mechanism are customized based on patient anatomy and are optimized based on the UNIPI dataset [22], to mimic the actual human index finger movements. In addition, the finger mechanism is driven by a micro linear actuator, which is mounted on the top of the opisthenar cover. The control board is attached to the forearm and no other external devices are required. The total weight of the finger mechanism is $45g$.

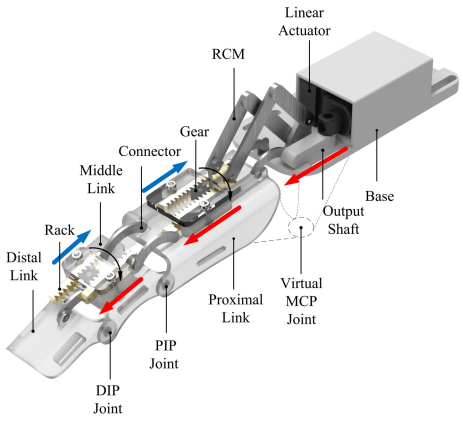

Figure 1. Overview of the index finger exoskeleton

The rest of the paper is organized as follows. Section 2 describes the design requirements of the finger exoskeleton mechanism. Section 3 presents the kinematic model of the exoskeleton. Section 4 introduces the optimization of the design variables. Section 5 presents the sensitivity analysis of the design variables. Section 6 describes the implementation of the proposed mechanism and analysis on the actual prototype. Section 7 concludes the paper.

2 FINGER MECHANISM DESIGN

The index finger exoskeleton consists of three links: a distal phalanx, a middle phalanx, and a proximal phalanx, as well as three relative joints, including a distal interphalangeal (DIP), a Proximal interphalangeal (PIP), and a metacarpophalangeal (MCP). The MCP joint has two DOFs, namely, the flexion–extension (up-down motion) and the abduction-adduction (sideways motion). For most of the grasping motions, the abduction and adduction mobility is achieved passively by the thenar eminence. Therefore, only the flexion-extension motion is considered for the MCP joint design. Due to the motion relationship between the anatomy of the adjacent joints, the finger can be simplified into one DOF bending motion.

Therefore, our goal is to design an index finger exoskeleton mechanism that focuses on restoring the grasping functionality for BPI patients with their ADLs and keeping a light, compact, and highly adaptable design. Based on the literature [7, 23–25], most of the existing finger exoskeletons consist of complicated linkage mechanisms, bulky actuators, and ponderous power supplies, which usually result in designs that are not portable for ADLs. By adapting the one DOF concept of the RCHM mechanism, our approach can overcome these shortcomings.

The main idea of RCHM is to transfer motions between adjacent links continuously around a joint using a rigid coupling mechanism, similar to a domino effect. However, one difference is that the RCHMs transfer the motion by a coupled mechanism between adjacent links. One of these coupled mechanisms is the rack and pinion mechanism, which is shown in Figure 2 where the second linkage does not connect with the input directly but is driven by the coupled motion of the rack and pinion mechanism. Moreover, the motion direction of the second linkage is based on the connection points, i.e., if the bottom rack of the second linkage connects with the output of the first linkage, the second linkage performs the same motion as the first linkage (red arrow); alternatively, if the top rack of the second linkage is connected to the output of the first linkage, the motion of the second linkage is in the opposite direction of the first linkage motion (blue arrow).

This characteristic can be utilized to design the finger exoskeleton since the phalanges' motion on the same finger are coupled during grasping. Figure 1 is the anatomical drawing of the finger exoskeleton showing the motion transmission from the motor to the fingertip, where the virtual MCP joint is implemented through a remote center of motion (RCM) mechanism.

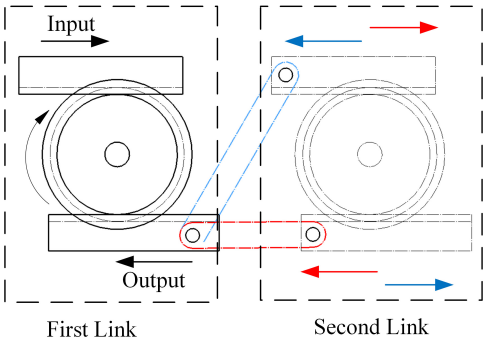

Figure 2. Example for 1 DOF of RCHMS and motion transmission between connected linkages.

The entire finger consists of serially connected offset slider-crank mechanisms and rack-pinion mechanisms. The motion begins with the linear actuator pushing the output shaft straightly forward. The output shaft, the connector between the output shaft and the Proximal link, the base, the virtual MCP joint, and the Proximal link form the first offset slider-crank mechanism, where the output shaft is the input and the virtual MCP joint is the output. Furthermore, the base, the connector between the base and Proximal link, the Proximal link, the virtual MCP joint, and the rack form the second offset slider-crank mechanism, with the virtual MCP joint being the input and the rack being the output. Due to the coupled motion of the first two slider-crank mechanisms, the motion of the linear actuator is transmitted to the motion of the first rack through driving the rotation of the virtual MCP joint. It is worth mentioning that the rack moves in the opposite direction (blue arrow) in comparison to the output shaft (red arrow). The rack and pinion mechanism joins in and reverses the motion direction from backward to forward. The rack, connector, Proximal link, PIP joint, and the middle link form the first offset slider-crank mechanism for the PIP joint. Similar to the motion sequence around the MCP joint, the PIP joint is driven by the rack on the proximal link. Continuing the motion transmission and the motion of the linear actuator is eventually transmitted to the end effector (Distal link). The offset slider-crank mechanism with forward motion (red arrow) is defined as the "Driving" mechanism because it drives the next linkage's motion. The offset slider-crank mechanism with backward movement (blue arrow) is defined as the "Measuring" mechanism because its motion is dependent on the "Driving" mechanism by measuring and copying the rotation angle of the "Driving" motion.

3 Index Finger Exoskeleton Kinematics

This section presents the kinematic model of the index exoskeleton finger for control, optimization, and sensitivity analysis. The equation of the forward kinematic chain is given by

$$p_x = l_p \cos\theta_{MCP} + l_m \cos(\theta_{MCP}+\theta_{PIP}) + l_d \cos(\theta_{MCP}+\theta_{PIP}+\theta_{DIP}) \quad (1)$$

$$p_y = l_p \sin\theta_{MCP} + l_m \sin(\theta_{MCP}+\theta_{PIP}) + l_d \sin(\theta_{MCP}+\theta_{PIP}+\theta_{DIP}) \quad (2)$$

where p_x and p_y are the position coordinates of the end point. l_p, l_m and l_d are the length of the proximal phalanx, middle phalanx and distal phalanx, respectively. θ_{MCP}, θ_{PIP} and θ_{DIP} are the joint angles of the MCP joint, PIP joint and the DIP joint, respectively.

The overall kinematics can be split into three sub-chains based on the joint location. Due to the similarity among the motions of the three joints, the PIP joint is selected to illustrate the sub kinematic chain for simplification. Figure 3 shows the full view of the rendered bent index exoskeleton finger and an enlarged view of the PIP joint. The Driving chain is marked using red color and the Measuring chain is marked using blue color, respectively. Considering that the rotation angle of the PIP joint (θ_{pip}) are the same in both chains, both models are established in the same coordinate (marked as black x, y and z). The travel distance of the rack in the Driving chain with respect to the rotation angle of the PIP joint can be expressed as:

$$d_{pip} = l_{pip,1} - \sqrt{l_{pip,1}^2 - (h_{pip} - \frac{h_{pip}\cdot\cos(\alpha_{pip,1}+\theta_{pip})}{\cos\alpha_{pip,1}})^2} - h_{pip}\cdot\tan\alpha_{pip,1} + \frac{h_{pip}\cdot\cos(\alpha_{pip,1}+\theta_{pip})}{\cos\alpha_{pip,1}} \quad (3)$$

where d_{pip} is the travel distance of the rack in the Driving chain. $l_{pip,1}$ is the link length of $\overline{D_{pip,a}D_{pip,b}}$. h_pip is the distance between the PIP joint and the middle plane of the rack. $\alpha_{pip,1}$ is the pre-rotation angle of link $\overline{D_{pip,b}S_{pip}}$ with respect to the z axis.

Similarly, the travel distance of the rack in the Measuring chain can be represented as:

$$d_{dip} = l_{pip,2} - \sqrt{l_{pip,2}^2 - (h_{pip} - \frac{h_2\cdot\cos(\alpha_{pip,2}+\theta_{pip})}{\cos\alpha_{pip,2}})^2} - h_{pip}\cdot\tan\alpha_{pip,2} + \frac{h_{pip}\cdot\cos(\alpha_{pip,2}+\theta_{pip})}{\cos\alpha_{pip,2}} \quad (4)$$

where d_{dip} is the travel distance of the rack in the Measuring chain. $l_{pip,2}$ is the link length of $\overline{M_{pip,a}M_{pip,b}}$. $\alpha_{pip,2}$ is the pre-rotation angle of link $\overline{M_{pip,a}S_{pip}}$ with respect to the z axis.

To simplify the problem, the same rack (Modulus=0.5mm) and pinion (Modulus=0.5mm, Teeth=10) combinations are chosen for each joint, which means that the travel distance of the slider in the current Measuring chain is the travel distance of the slider in the next Driving chain. Generalizing the above analy-

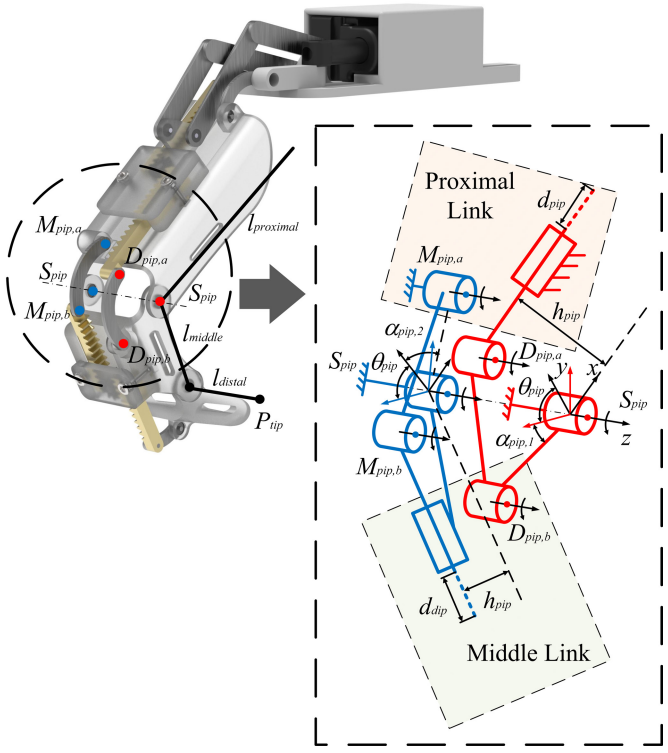

Figure 3. Full view of bent index exoskeleton finger and kinematic model of the PIP joint

sis to the MCP joint and the DIP joint, another three equations about rotation angles with respect to the rack travel distances can be derived as:

$$d_{mcp} = l_{mcp,1} - \sqrt{l_{mcp,1}^2 - (h_{mcp} - \frac{h_{mcp}\cdot\cos(\alpha_{mcp,1}+\theta_{mcp})}{\cos\alpha_{mcp,1}})^2} - h_{mcp}\cdot\tan\alpha_{mcp,1} + \frac{h_{mcp}\cdot\cos(\alpha_{mcp,1}+\theta_{mcp})}{\cos\alpha_{mcp,1}} \quad (5)$$

$$d_{pip} = l_{mcp,2} - \sqrt{l_{mcp,2}^2 - (h_{mcp} - \frac{h_{mcp}\cdot\cos(\alpha_{mcp,2}+\theta_{mcp})}{\cos\alpha_{mcp,2}})^2} - h_{mcp}\cdot\tan\alpha_{mcp,2} + \frac{h_{mcp}\cdot\cos(\alpha_{mcp,2}+\theta_{mcp})}{\cos\alpha_{mcp,2}} \quad (6)$$

$$d_{dip} = l_{dip,1} - \sqrt{l_{dip,1}^2 - (h_{dip} - \frac{h_{dip}\cdot\cos(\alpha_{dip,1}+\theta_{dip})}{\cos\alpha_{dip,1}})^2} - h_{dip}\cdot\tan\alpha_{dip,1} + \frac{h_{dip}\cdot\cos(\alpha_{dip,1}+\theta_{dip})}{\cos\alpha_{dip,1}} \quad (7)$$

where θ represents the rotation angle with respect to the corresponding joint, α represents the pre-rotation angle of the corresponding joint, h represents the distance between the corresponding joint and the corresponding middle plane of the rack, l represents the link length of different phalanges, and d represents the travel distance of racks with respect to the corresponding joints. The first subscript denotes the current joint and the second subscript denotes the current chain (1 for Driving and 2 for Measuring). With the input (the travel distance) from the linear actuator, the output (the corresponding fingertip position) can be calculated.

4 OPTIMIZATION OF DESIGN VARIABLES

In order to imitate the human hand index finger motion, optimization of the design variables is conducted. To get better performance, each joint axis on the exoskeleton should coincide with the joint axis on the human finger. Due to the large size and shape variations for individual human fingers, the optimization is performed using the author's finger dimensions as an example, which can be found in Table 1. The feasibility of designing for different finger sizes will be discussed in Section 6.

Table 1. Length of Each Phalanx

Phalanx Name	Length (mm)
Proximal	50.0
Middle	27.2
Distal	26.4

Due to its high performance, the UNIPI dataset [22] is chosen as the standard motion for the optimization. Because of the limited DOF of the index exoskeleton, the desired grasping motion path should allow the exoskeleton to grasp as many objects as possible, which means the desired grasping motion path should cover a large workspace. The hand joint data of grasping the No. 8 object with respect to the No.1 subject is selected based on the above criterion. Each path includes thousands of position data points and each position data point consists of the angle information of each joint. However, there are overlaps among the data points since the data recorded includes both the grasping and the releasing motion. Therefore, the data is first pre-processed to contain only the grasping motion. We picked six positions that are equally distributed on the path as the landmarks. The objective function for optimization is the root mean square error ($\mathbf{e}$) between the joint angles on the exoskeleton and the joint angles on the landmarks, with different weight ($\mathbf{w_{1\sim6}}$) for each position,

$$F(x) = [\mathbf{w_1} \quad \mathbf{w_2} \quad \mathbf{w_3} \quad \mathbf{w_4} \quad \mathbf{w_5} \quad \mathbf{w_6}]_{1\times18}[\mathbf{e}]_{18\times1} \quad (8)$$

Equations (3)~(7) form the nonlinear equality constraints of the optimization. The following nonlinear inequality constraints should be added too to guarantee that the rack and pinion mechanism works properly.

$$2 \cdot d_{mcp} \leq l_{proximal} - h_{mcp} \cdot \cos(\alpha_{mcp,1}) - h_{pip} \cdot \cos(\alpha_{pip,2}) \quad (9)$$

$$2 \cdot d_{pip} \geq l_{intermediate} - h_{pip} \cdot \cos(\alpha_{pip,1}) - h_{pip} \cdot \cos(\alpha_{dip,2}) \quad (10)$$

$$h_{pip} \leq h_{mcp} \quad (11)$$

$$h_{dip} \leq h_{pip} \quad (12)$$

Considering the following different motion range of each joint and the relationship between the adjacent joints [26]:

$$0^\circ \leq \theta_{mcp} \leq 90^\circ \quad (13)$$

$$0^\circ \leq \theta_{pip} \leq 110^\circ \quad (14)$$

$$0^\circ \leq \theta_{dip} \leq 90^\circ \quad (15)$$

$$\theta_{dip} = \frac{2}{3}\theta_{pip} \quad (16)$$

we chose the weights ($w_{joint} = [1, 2, 1]$) for each of the three joints and equal weights for different positions. The optimized design variables are listed in Table 2.

Table 2. Optimized design variables

Variable	Value	Variable	Value
$l_{mcp,1}$	13.0 mm	$l_{mcp,2}$	13.9 mm
$l_{pip,1}$	15.0 mm	$l_{pip,2}$	15.6 mm
$l_{dip,1}$	8.2 mm	h_{mcp}	16.7 mm
h_{pip}	10.0 mm	h_{dip}	10.0 mm
$\alpha_{mcp,1}$	17.1 deg	$\alpha_{mcp,2}$	22.3 deg
$\alpha_{pip,1}$	24.6 deg	$\alpha_{pip,2}$	30.0 deg
$\alpha_{dip,1}$	30.0 deg		

Figure 4 shows the trajectory comparison results between the standard human index finger (from UNIPI dataset) and our index finger exoskeleton. The results show that the optimized trajectory of the exoskeleton follows the index finger trajectory consistently. The error comes from the DOF differences between the exoskeleton and the actual index finger. For the human finger, some joints achieve the final angle faster than others and thus stop moving earlier. However, the joints on the exoskeleton finger move and stop together due to the single DOF design. The results also show that the exoskeleton finger has a larger range of motion which enables the exoskeleton to grasp smaller objects after optimization.

5 SENSITIVITY ANALYSIS

Sensitivity analysis is an important component of post-processing. It is the key to understand the effects of the design variables. For the index finger exoskeleton design, there are thirteen design variables ($\boldsymbol{\Theta}$), as listed in Table 2. Based on the constraint equations (Eqns. 1~7) derived in Section 3, the sensitivity of the index finger exoskeleton is given by

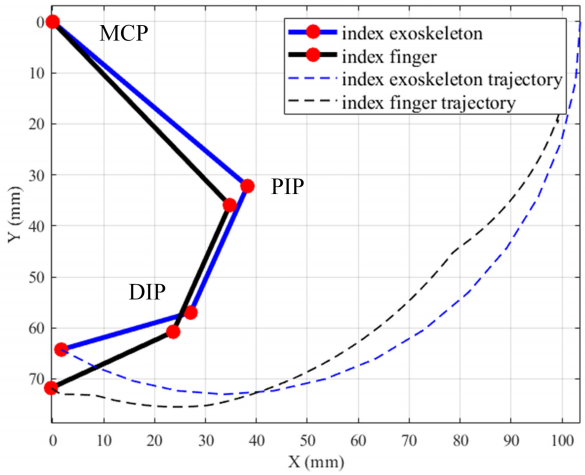

Figure 4. Comparison between index finger motion and index exoskeleton trajectory, and bending angles of the joints.

$$[\dot{\mathbf{p}}]_{2\times1} = [\mathbf{J}]_{2\times13}[\dot{\boldsymbol{\Theta}}]_{13\times1} \quad (17)$$

$$\mathbf{J} = \begin{bmatrix} \frac{\partial \mathbf{p}}{\partial l_{mcp,1}} & \frac{\partial \mathbf{p}}{\partial l_{mcp,2}} & \frac{\partial \mathbf{p}}{\partial l_{pip,1}} & \frac{\partial \mathbf{p}}{\partial l_{pip,2}} & \frac{\partial \mathbf{p}}{\partial l_{dip,1}} \\ \frac{\partial \mathbf{p}}{\partial \alpha_{mcp,1}} & \frac{\partial \mathbf{p}}{\partial \alpha_{mcp,2}} & \frac{\partial \mathbf{p}}{\partial \alpha_{pip,1}} & \frac{\partial \mathbf{p}}{\partial \alpha_{pip,2}} & \frac{\partial \mathbf{p}}{\partial \alpha_{dip,1}} \\ \frac{\partial \mathbf{p}}{\partial h_{mcp}} & \frac{\partial \mathbf{p}}{\partial h_{pip}} & \frac{\partial \mathbf{p}}{\partial h_{dip}} \end{bmatrix} \quad (18)$$

where $\dot{\mathbf{p}} = [\dot{p_x}, \dot{p_y}]^T$ represents the velocity vector at the end of the fingertip, $\mathbf{J}$ represents the Jacobian of the system and $\dot{\boldsymbol{\Theta}}$ represents the derivatives of the design variables. The numerical differentiation method is implemented to calculate $\mathbf{J}$. Twenty configurations of the system have been selected based on the isometric traveling distance of the linear actuator (d_{mcp}) from the beginning to the end. Figure 5 shows the sensitivity of each variable at each configuration. The influence of each design variable on the fingertip position is increased with the fingertip reaching the end position. Also, the design variables around the PIP joint have a larger influence on the fingertip position in comparison to other joints.

6 EXPERIMENTS AND DISCUSSION

The proposed novel index finger exoskeleton aims to provide a compact and portable design for the wearable devices that help with daily activities of the patients. Based on the opti-

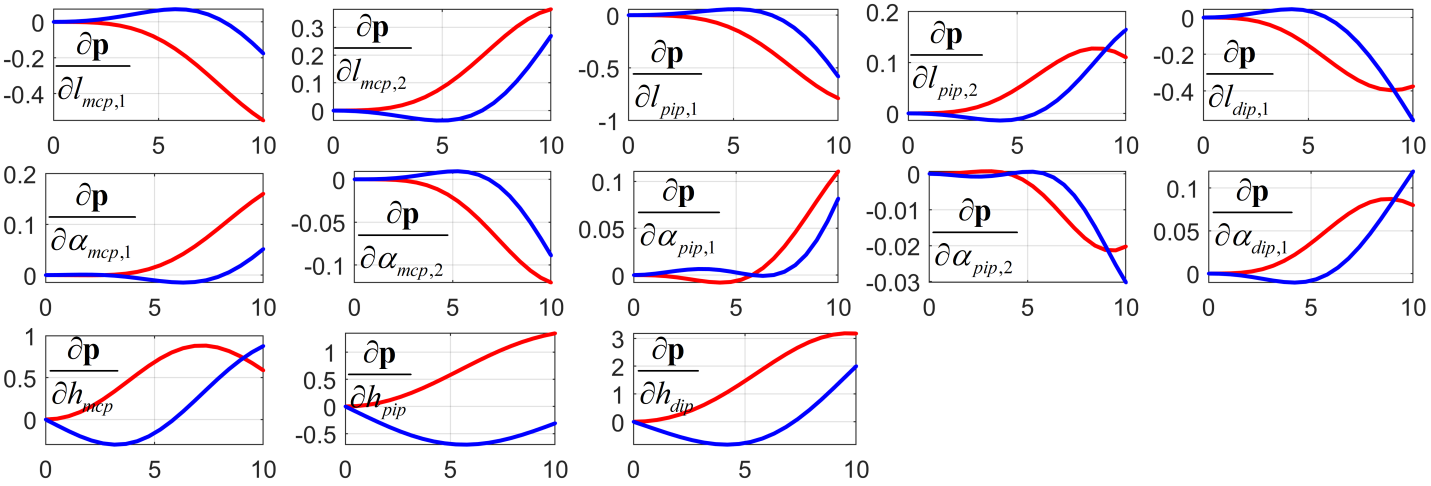

Figure 5. Sensitivity analysis of each design variable. The Red lines refer to the sensitivity for the x component of **p** and the blue lines refer to the y component.

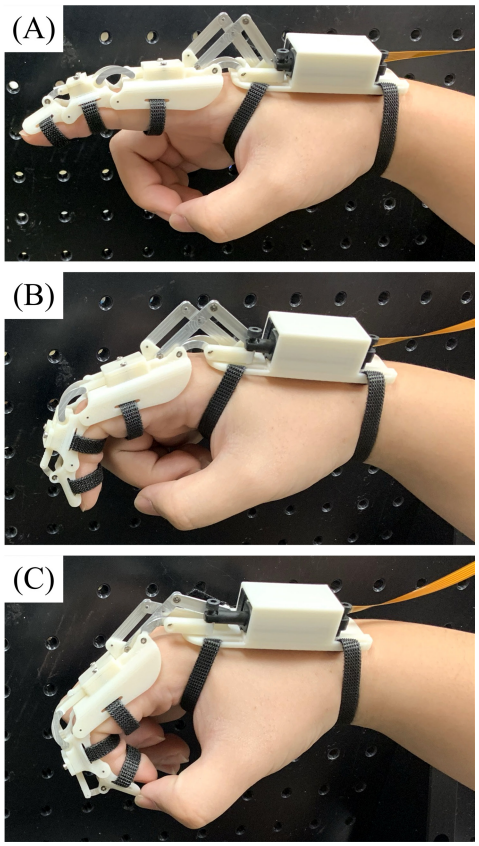

Figure 6. Motion experiments with the index exoskeleton finger. (A) Side view of the initial position. (B) Side view of the position during the motion. (C) Side view at the end of the motion

mization result in Section 4, a prototype was built to verify the mechanism mobility. The shell, rack, and pinion are made out of Acrylonitrile Butadiene Styrene (ABS) through 3D printing. The connectors are made out of aluminum. The Actuonix micro linear actuator PQ12 was chosen due to its small dimension, light weight, and a relatively large output force of 50N. The total weight of the exoskeleton is 45g. Velcro straps were used to fasten the device on each phalanx.

Figure 6 shows the motion from the initial position to the final position. The trajectory follows the optimization results. Considering the thickness of the finger, a small object with a diameter of around 30mm can be held. Other team members with similar finger dimensions also tested the exoskeleton and it showed that even in situations where the joints were not perfectly aligned with the finger joints, the mechanism still worked well due to the soft connection between the exoskeleton and human finger via Velcro straps.

However, potential problems associated with the proposed index finger exoskeleton were also identified. Due to the long kinematic chain, the errors on each design variable were accumulated, which affected the motion of the fingertip. In addition, because there are several sliding parts, it is difficult to find a balance between reducing the kinetic friction and minimizing the backlash. Moreover, because of the large motion range of the PIP joint, the offset slider-crank mechanism could easily move close to a singular position. Overcoming these drawbacks will be a major focus of future work. Further research on the force control and the development of the entire hand mechanism is also the focus of our future work.

7 CONCLUSION

In this paper, we presented a novel mechanism to build a functional, compact, and portable index finger exoskeleton for individuals with hand disabilities, to assist their activities of daily living and rehabilitation. Mechanical design and kinematic analysis of the novel mechanism were presented first and an optimization for a better alignment with the actual index finger's motion was then conducted. The optimized exoskeleton achieved a similar motion as a human finger for grasping small objects. In addition, a sensitivity analysis for each design variable was performed to analyze the influence of each design variable on the fingertip position accuracy. The index finger exoskeleton experiments demonstrate the new mechanism's ability to grasp small objects with dexterity. Moreover, the motor is mounted on the back of the hand in a manner such that the exoskeleton does not require any external actuation.

ACKNOWLEDGMENT

Research reported in this publication was supported by the Eunice Kennedy Shriver National Institute of Child Health & Human Development of the National Institutes of Health under Award Number R21HD095027. The content is solely the responsibility of the authors and does not necessarily represent the official views of the National Institutes of Health.

REFERENCES

[1] Fujikawa, K., 1963. "The Center of Gravity in the Parts of Human Body". *Okajimas Folia Anatomica Japonica,* ***39***(3), pp. 117–125.

[2] Park, H. R., Lee, G. S., Kim, I. S., and Chang, J.-C., 2017. "Brachial Plexus Injury in Adults". *The Nerve,* ***3***(1), pp. 1–11.

[3] Giuffre, J. L., Kakar, S., Bishop, A. T., Spinner, R. J., and Shin, A. Y., 2010. "Current Concepts of the Treatment of Adult Brachial Plexus Injuries". *Journal of Hand Surgery,* ***35***(4), 4, pp. 678–688.

[4] Carmeli, E., Peleg, S., Bartur, G., Elbo, E., and Vatine, J. J., 2011. "HandTutorTM enhanced hand rehabilitation after stroke - a pilot study". *Physiotherapy Research International,* ***16***(4), pp. 191–200.

[5] Wolf, S. L., Winstein, C. J., Miller, J. P., and Morris, D., 2006. "Effect of Constraint-Induced Movement". pp. 2095–2104.

[6] Takahashi, C. D., Der-Yeghiaian, L., Le, V., Motiwala, R. R., and Cramer, S. C., 2008. "Robot-based hand motor therapy after stroke". *Brain,* ***131***(2), pp. 425–437.

[7] Bos, R. A., Haarman, C. J., Stortelder, T., Nizamis, K., Herder, J. L., Stienen, A. H., and Plettenburg, D. H., 2016. "A structured overview of trends and technologies used in dynamic hand orthoses". *Journal of NeuroEngineering and Rehabilitation,* ***13***(1), pp. 1–25.

[8] Borboni, A., Mor, M., and Faglia, R., 2016. "Gloreha-Hand Robotic Rehabilitation: Design, Mechanical Model, and Experiments". *Journal of Dynamic Systems, Measurement and Control, Transactions of the ASME,* ***138***(11), 11.

[9] Orihuela-Espina, F., Roldán, G. F., Sánchez-Villavicencio, I., Palafox, L., Leder, R., Sucar, L. E., and Hernández-Franco, J., 2016. "Robot training for hand motor recovery in subacute stroke patients: A randomized controlled trial". *Journal of Hand Therapy,* ***29***(1), 1, pp. 51–57.

[10] Polygerinos, P., Wang, Z., Galloway, K. C., Wood, R. J., and Walsh, C. J., 2015. "Soft robotic glove for combined assistance and at-home rehabilitation". *Robotics and Autonomous Systems,* ***73***, pp. 135–143.

[11] Kudo, S., Oshima, K., Arizono, M., Hayashi, Y., and Moromugi, S., 2014. "Electric-powered glove for CCI patients to extend their upper-extremity function". In 2014 IEEE/SICE International Symposium on System Integration, SII 2014, Institute of Electrical and Electronics Engineers Inc., pp. 638–643.

[12] Deimel, R., and Brock, O., 2016. "A novel type of compliant and underactuated robotic hand for dexterous grasping". *The International Journal of Robotics Research,* ***35***(1-3), 1, pp. 161–185.

[13] Ilievski, F., Mazzeo, A. D., Shepherd, R. F., Chen, X., and Whitesides, G. M., 2011. "Soft Robotics for Chemists". *Angewandte Chemie,* ***123***(8), 2, pp. 1930–1935.

[14] Yap, H. K., Ang, B. W., Lim, J. H., Goh, J. C., and Yeow, C. H., 2016. "A fabric-regulated soft robotic glove with user intent detection using EMG and RFID for hand assistive application". In Proceedings - IEEE International Conference on Robotics and Automation, Vol. 2016-June, Institute of Electrical and Electronics Engineers Inc., pp. 3537–3542.

[15] Ma, Z., Ben-Tzvi, P., and Danoff, J., 2015. "Sensing and Force-Feedback Exoskeleton Robotic (SAFER) Glove Mechanism for Hand Rehabilitation". *Proceedings of the ASME Design Engineering Technical Conference,* ***5A-2015***, pp. 1–8.

[16] Aiple, M., and Schiele, A., 2013. "Pushing the limits of the CyberGrasp™ for haptic rendering". *Proceedings - IEEE International Conference on Robotics and Automation*, pp. 3541–3546.

[17] Hofmann, U. A., Bützer, T., Lambercy, O., and Gassert, R., 2018. "Design and Evaluation of a Bowden-Cable-Based Remote Actuation System for Wearable Robotics". *IEEE Robotics and Automation Letters,* ***3***(3), pp. 2101–2108.

[18] Leonardis, D., Barsotti, M., Loconsole, C., Solazzi, M., Troncossi, M., Mazzotti, C., Castelli, V. P., Procopio, C., Lamola, G., Chisari, C., Bergamasco, M., and Frisoli, A., 2015. "An EMG-controlled robotic hand exoskeleton for

bilateral rehabilitation". *IEEE Transactions on Haptics,* ***8***(2), pp. 140–151.

[19] Ho, N. S., Tong, K. Y., Hu, X. L., Fung, K. L., Wei, X. J., Rong, W., and Susanto, E. A., 2011. "An EMG-driven exoskeleton hand robotic training device on chronic stroke subjects: Task training system for stroke rehabilitation". In IEEE International Conference on Rehabilitation Robotics.

[20] Liu, Y., and Ben-Tzvi, P., 2020. "A new extensible continuum manipulator using flexible parallel mechanism and rigid motion transmission". *Proceedings of the ASME Design Engineering Technical Conference,* ***10***.

[21] Liu, Y., and Ben-Tzvi, P., 2020. "Design, Analysis, and Integration of a New Two-Degree-of-Freedom Articulated Multi-Link Robotic Tail Mechanism". *Journal of Mechanisms and Robotics,* ***12***(2), pp. 1–9.

[22] Della Santina, C., Bianchi, M., Averta, G., Ciotti, S., Arapi, V., Fani, S., Battaglia, E., Catalano, M. G., Santello, M., and Bicchi, A., 2017. "Postural hand synergies during environmental constraint exploitation". *Frontiers in Neurorobotics,* ***11***(August), pp. 1–14.

[23] Heo, P., Gu, G. M., Lee, S. j., Rhee, K., and Kim, J., 2012. "Current hand exoskeleton technologies for rehabilitation and assistive engineering". *International Journal of Precision Engineering and Manufacturing,* ***13***(5), pp. 807–824.

[24] Platz, T., 2003. "Evidenzbasierte armrehabilitation: Eine systematische literaturü bersicht". *Nervenarzt,* ***74***(10), pp. 841–849.

[25] Xu, W., Pradhan, S., Guo, Y., Bravo, C., and Ben-Tzvi, P., 2020. "A Novel Design of a Robotic Glove System for Patients With Brachial Plexus Injuries". *Proceedings of the ASME Design Engineering Technical Conference,* ***10***, 11.

[26] Lin, J., Wu, Y., and Huang, T. S., 2000. "Modeling the constraints of human hand motion". *Proceedings - Workshop on Human Motion, HUMO 2000*, pp. 121–126.